Highly Compact Twin 1×35 Wavelength Selective Switch

Z. Huang, S. Yang, Z. Zheng, X. Pan, H. Li and H. Yang

***Abstract*—This paper demonstrates the design, assembly, optimisation and characterisation of a twin 1×35 wavelength selective switches (WSSs) based on a highly dispersive silicon grating prism (GRISM). The footprint of this WSS is reduced by >50% when compared with the standard module, without sacrificing key performance metrics including insertion loss, spectral coverage, passband, isolation, etc. To our knowledge, this module is the most compact high port count WSS demonstrated so far.**

***Index Terms*—Wavelength Selective Switch, Liquid crystal on silicon**

I. Introduction

Reconfigurable optical add/drop multiplexers (ROADMs) [1]–[3] have transformed the modern telecommunication networks [4] and datacentre interconnect (DCI) networks [5] into a highly interconnected, reconfigurable photonic mesh. In the ROADM networks, operators are able to route all the wavelength-division multiplexed (WDM) signals entirely in the optical domain without the need for optical-electrical-optical (OEO) conversion. This eliminated the highly power-hungry process of optical-electrical-optical (OEO) conversion used in the traditional routers. State-of-the-art ROADMs also support the flexible grid standard [6], where wavelength channels are not constrained to the fixed ITU channels slots. This enables more efficient use of the spectrum available within the ROADM networks and therefore maximises the total network capacity. The support for the flexible grid standard and the nature of all optical switching also makes the ROADMs compatible with any future signal modulation formats. As a result, the ROADMs are expected to be in service for more than a decade once they are deployed. This saves the capital expenses (CapEx) for the network operators in the long run. The reconfiguration of a ROADM can be done remotely by software, which further reduces the operational expenses (OpEx).

Latest generation of ROADM systems are based on the 'route-and-select' architecture [7], in which multiple wavelength selective switches (WSSs) [8]–[10] are paired with each other at the transit side to enable the cross-connecting of WDM channels between different ROADM degrees. At each ROADM degree, a pair of WSSs are deployed, one for the incoming fibre and the other for the outgoing fibre. Therefore, a typical eight-degree ROADM consists of 16 WSSs. As the Internet traffic continues to grow exponentially, the network evolves towards increasingly meshed topologies, driving the ROADMs to even higher degrees. In order to maintain the overall cost of ROADMs, there is a strong demand for WSSs with reduced footprint and cost but increased port count.

Co-packaging multiple WSS systems into a single module is an effective way to reduce the cost of WSSs while increasing the switching density. At the transit side, twin WSS modules [11], which integrated two independent WSSs with a port count up to 32, have been commercialised and are widely deployed in the modern ROADMs. A twin WSS module is able to handle both the incoming and outgoing fibres of a ROADM degree. Recently, quad-WSS modules [12] have also become available. This type of module is able to deliver all the WSSs required for the transit side of a two-degree ROADM. However, it may also create a single point of failure in a ROADM node. Further integration is possible. Yang et al. [13], [14] successfully co-packaged 24 independent 1×12 WSSs into a single module. For the add/drop part of the ROADMs, co-packaged WSS modules are able to provide highly scalable and low loss colourless, directionless and contentionless (CDC) [15] solutions. This type of wavelength crossconnect (WXC) architecture was first proposed in [16]. The first practical demonstration was done by Ikuma et al., in which eight independent 1×24 WSSs and 24 1×8 space switches were integrated to realise an 8×24 WXC [17], [18]. The relatively high insertion loss in those demonstrations was significantly reduced by Colbourne et al [19].

The footprint of either single or co-packaged WSS modules largely depends on the dispersing capability of the DEMUX element required in its optical system. In majority of the WSS demonstrations, a diffraction grating and a prism are bonded together to form a GRISM as the DEMUX element. Standard GRISM based on the glass materials can deliver a dispersion of ~0.15 degree/nm over the C-band wavelengths. Marom et al. [20] demonstrated a WSS system based on a highly dispersive arrayed waveguide (AWG) device. Virtually imaged phase array (VIPA) used in a recent WSS demonstration [21] are also more dispersive than the standard GRISM. However, the free spectral range (FSR) of these dispersive components cannot

Manuscript received July 20, 2022.

Z. Huang, S. Yang, and H. Yang, are with Display R&D Centre, Southeast University, Nanjing 210096, China (e-mail: h.yang@seu.edu.cn)

Z. Zheng, X. Pan and H. Li are with Huawei Technologies Company, Ltd., Shenzhen 518129, China

cover the whole C band. This will further limit the spectral coverage of the WSS module.

In this work, we demonstrate a compact twin 1×35 WSS system based on a highly dispersive silicon GRISM component. The customised GRISM was able to achieve a dispersion of ~0.4 degree/nm, without introducing excessive optical aberrations. As a result, the footprint of this twin WSS module was reduced by >50% when compared with the standard modules based on the glass GRISM. The performance of our WSS module can be maintained at the same level. This paper will detail the design, assembly, optimisation and characterisation of this WSS system.

II. System Design and Assembly

A. LCOS SLM

A Liquid crystal on silicon (LCOS) [22] spatial light modulator (SLM) was used as the switching engine in this work due to its support for flexible spectrum switching [23]. The system was specifically designed for a phase-only LCoS device that has an active area of 1920×1200 pixels and a pixel pitch of 8 µm. The device employs an analogue voltage driving scheme and is capable of resolving 256 discrete phase levels with a maximum modulation of 2.5π at 1550 nm. The extremely low phase flicker [24], [25] of this LCOS device can help minimise the crosstalk within the WSS [26]. Anti-reflection coating and index matching are implemented. The reflectance of this LCOS device was measured to be >87% across the whole C band, with a ripple less than 0.3 dB. This would introduce minimum insertion loss to the WSS module and ensure a uniform passband performance across the designed spectrum range.

B. Optical Architecture

The optical architecture of the switch module is shown in Fig. 1. The architecture is split into two sections: the switching optics and the relay optics. The switching optics contains a pair of linear fibre arrays along the x-axis, which is also the switching axis of this WSS module. These two fibre arrays are monotonically fabricated on a single substrate with a pitch of 4.8 mm. They correspond to the two WSSs integrated within this module. Within each fibre array, the 36 single-mode fibres are arranged linearly on a 90 µm. The mode field diameter of these fibres with a reduced diameter of 80 µm is ~9.6 µm. A linear silicon collimating lenslet array is attached to these fibre arrays to slow down the divergence of the optical beams launched into the free space. As a result, the fibre ports have an effective mode field diameter of ~46 µm at their output planes. As shown in Fig. 1, the switching optics follows a *2f* arrangement along the x-axis and a *4f* arrangement along the y-axis. The cylindrical lens array (CL_{S1}) with a focal length of 50 mm is used as a Fourier lens to image the input beams from the two WSSs to its back focal plane (P_o). At Plane Po, the Gaussian beam waist is converted to 1.07 mm along the x-axis. Along the y-axis, two cylindrical lenses, CL_{W1} and CL_{W2}, constitute a 1:1 optical relay system that images the fibre ports to Plane P_o. Therefore, the input optical beam will have a Gaussian beam waist of 23 µm along the y-axis at Plane P_o. The amorphic configuration of the switching optics produces elongated beam profiles at Plane P_o. This helps maximising the port count and passband performance of the WSSs.

Plane P_o is also the interface to the relay system. This is a symmetric *4f* relay, consisting of two lenses (L_1 and L_2) with focal lengths of ~45 mm, and a silicon GRISM DEMUX placed at the back focal plane of L_1. The details about this silicon GRISM will be introduced in the next section. The relay system essentially images the plane P_o onto the LCOS SLM. A Wollaston prism is placed at Plane P_o to impart angular difference between the two orthogonal polarisations (the solid line and the dashed line). A half-wave plate is placed within the optical path of one polarisation so that both beams are aligned with the operational polarisation direction of the DEMUX and the LCOS device. After passing through L_1, the dashed and solid beams shown in Fig. 1 hit the DEMUX with the same polarisation state and the same angle. Since the DEMUX imparts an angular displacement to each wavelength channel in

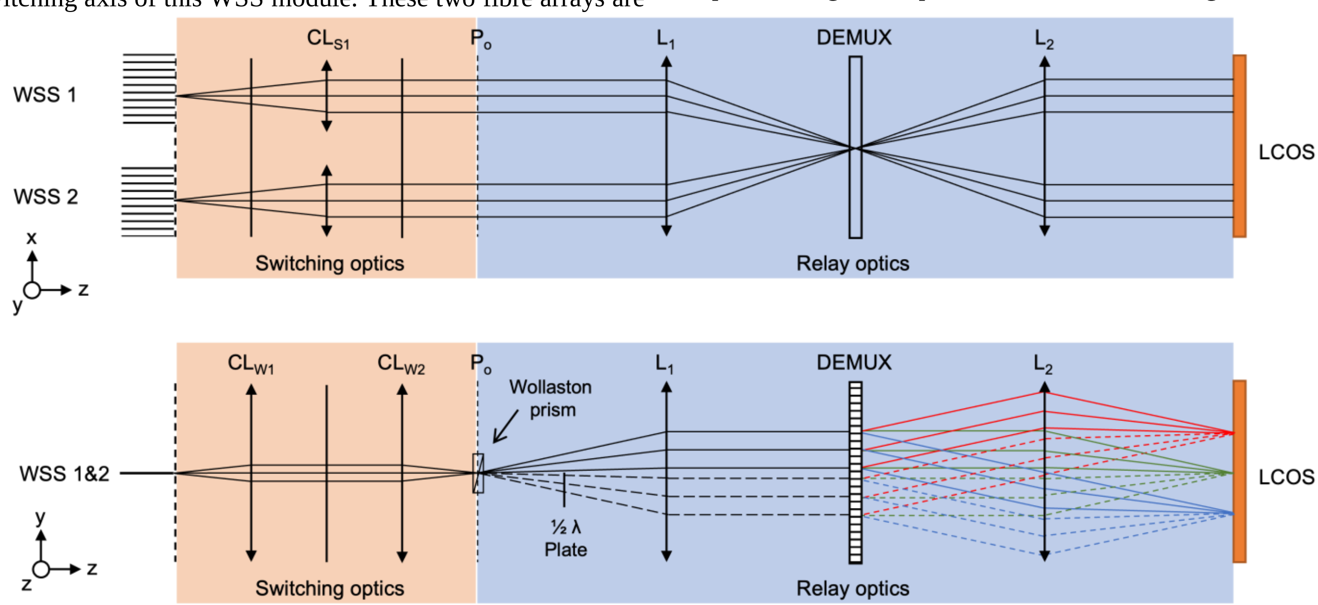

Fig. 1. The optical architecture of stacked WSS module

the y-z plane, the input WDM signals from each WSS will illuminate a spatially distinct row of sub-holograms. The y-axis is hence referred to as the dispersion axis. Sub-hologram rows for two WSSs are separated by 4.8 mm, i.e. 600 pixels along the y-axis.

It should be noted that the dashed and solid beams for each wavelength are recombined at the LCOS plane. Since they also have the opposite incident angle to the LCOS device along the y-z plane, they will retrace each other on the way back. This polarisation diversity scheme enables us to construct a polarisation insensitive WSS system based on the polarisation sensitive optical components, i.e. GRISM and the LCOS device.

The unmodulated input beam covers 401.25×8.625 pixels on the LCOS device. Adjacent 50 GHz channels are separated by 12.5 pixels in the y-axis. This translated to a theoretical -0.5 dB passband width of >33 GHz for a 50 GHz channel [27]. There are 1920 pixels available along the y-axis of the LCOS device, so the module can cover >7500 GHz of spectrum in theory. However, the optical aberration will be larger for the edge wavelengths, leading to a higher insertion loss for those wavelength channels. The designed spectral range of this specific module ranges from 190.20 THz to 195.15 THz, i.e. ~100 50 GHz WDM channels. It should be noted that each pixel column in the sub-holograms corresponds to 4 GHz spectrum. However, the passband width of this system can be tuned with significantly higher resolution by using the sub-column technique, if required.

Each sub-hologram will encode a wavefront pattern in the form of blazed gratings to the beam of the corresponding wavelength channel, along the x-axis. This will be subsequently imaged back to plane Po by the relay optics. Given the telecentric arrangement of the switching optics along the x-axis, the CL_{S1} associated with each WSS will convert the encoded wavefront tilts to positional offsets with respect to the local input optical axis. The wavefront tilts imparted by the sub-hologram are only along the x-axis, corresponding to the linear arrangement of the fibre ports.

In this specific demonstration module, two independent 1×35 WSSs are implemented. However, the WSS count and the port count can be reconfigured for different applications without changing the design of the relay optics. For example, the current 1×2 CL_{S1} array can be replaced by a 1×4 array with a reduced focal length. This will enable a quad WSS configuration although the port count of each WSS needs to be reduced.

C. Silicon GRISM

Fig. 2 shows the general design of the silicon GRISM used in this work. A silicon grating with a groove density of 3200 lines/mm is bonded to the back surface of a silicon prism. An SEM image of the groove profile is given in Fig. 3. The apex angle of the silicon prism is designed a 53.25°. When the incident angle to the silicon grating surface is set close to its Littrow angle, this GRISM component is able to have a dispersion of 0.3 degree/nm over the C-band. It should be noted that the standard glass GRISM [28] used in the most of the WSS modules [29],[30] has a groove density of ~1200 lines/mm and a dispersion capability of <0.2 degree/nm. Therefore, this silicon GRISM with a doubled dispersion capability allowed us to reduce the focal length of L2 by >30%, leading to a ~50% reduction in the footprint of the WSS optical system.

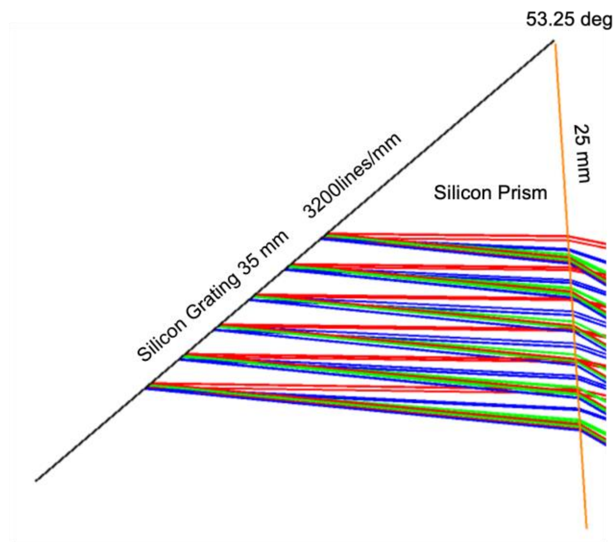

Fig. 2. Silicon GRISM design

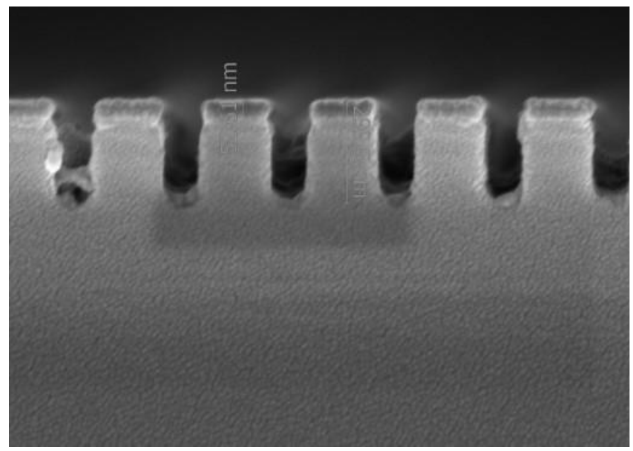

Fig. 3. Silicon GRISM design

Since the silicon has a high refractive index of ~3.5, the silicon prism is able to significantly reduce the optical beam's incident angle to the grating surface along the x-z plane. This helps to minimise the conical diffraction [31], [32], i.e. out of plane diffraction, of the silicon grating. The conical diffraction effect of the diffraction grating will produce crescent beam shapes on the LCOS device that could worsen the passband and insertion loss performance of the WSS module. Fig. 4 gives a comparison of beam shapes of different wavelengths on the LCOS device when a standard glass GRISM and a silicon GRISM are used, respectively. For a fair comparison, both GRISMs have a dispersion capability of 0.3 degree/nm although the groove density of the glass grating is only 1800 lines/mm due to its lower refractive index. It can be seen that the beam profiles on the LCOS device are severely distorted when the glass GRISM is used. However, the silicon GRISM can still produce standard elliptical beam profiles on the LCOS device.

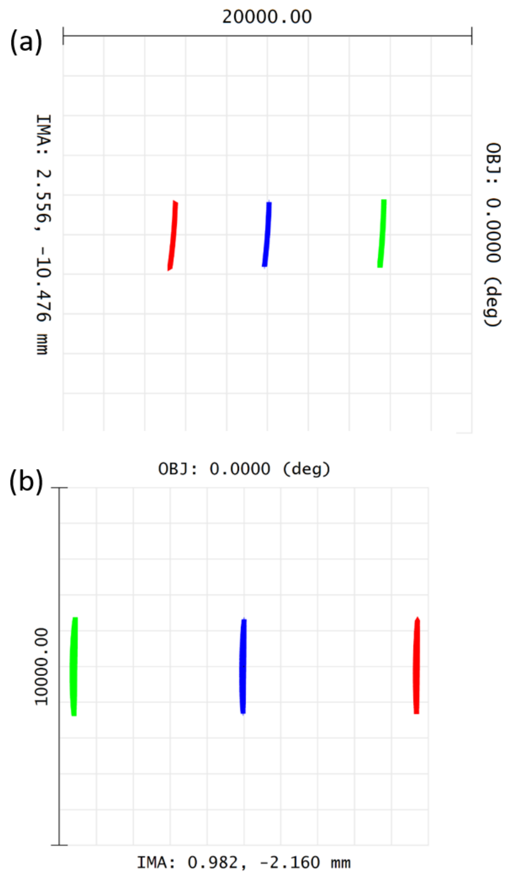

Fig. 4. Beam profiles on the LCOS plane: (a) using standard glass GRISM; (b) using silicon GRISM

The fabricated GRISM used in this work was polarisation sensitive and was measured to have a diffraction efficiency of 87% – 92% across the C band for the target polarisation state. This level of diffraction efficiency was comparable with the state-of-art glass GRISMs. Therefore, it would not introduce extra insertion loss penalty.

D. Assembly

The assembly of WSS systems is always extremely challenging as it requires sub micrometre precision over a relatively long optical path. Fig. 5 shows the experimental implementation of our twin 1×35 WSS module based on the architecture shown in Fig. 1. A curved mirror, i.e. the main lens in Fig. 5, was used to act as both the L_1 and L_2 in Fig. 1. This folded the relay optics and reduced its footprint. This curved mirror had a focal length of ~45 mm, which was >30% shorter than the focal length of the main lens used in the standard WSS modules [29], [30]. As a result, this helped to reduce the footprint of the relay optics by >50%. For the proof-of-concept demonstration, the switching optics was not folded in the current implementation. However, it can be expected that a single mirror folding of the switching optics is able to reduce the footprint to less than 50 mm by 50 mm.

It should be noted that there were a few additional optical components in the actual implementation. They were mainly responsible for the aberration compensation and beam

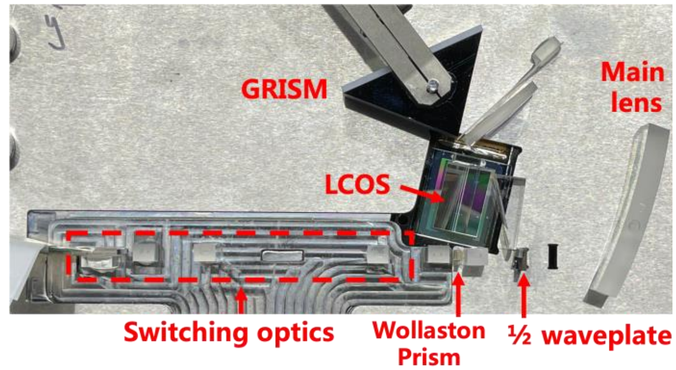

Fig. 5. The experimental setup of the twin 1×35 WSS module

conditioning. The overall optical architecture still followed Fig. 1. The maximum clear aperture required for the optical components within this system was maintained <10 mm along the *x*-axis.

III. Experimental Results

The performance of this demonstration was extensively characterised for its insertion loss, crosstalk, and passband, as the key WSS metrics that determine the performance of ROADM networks [33]–[36]. This section will present the detailed characterisation results of our compact twin 1×35 WSS module.

A. Insertion loss

The insertion loss of this demonstration system was measured across the whole supported wavelength range for all the output ports of each WSS. In this measurement, the width of the sub-holograms was set at ~9 pixels, which corresponded to three times of the waist of an un-modulated optical beam on the LCOS plane. The experimental results are presented in Table I. The measured insertion loss level ranges from 4.65 dB

TABLE I
Performance of the WSSs

	Min	Typical	Max
Insertion loss (dB)	4.65	5.96	7.2
Polarisation dependent loss (dB)			0.3
Insertion loss variation across the spectrum (dB)			±1.0
Inter-WSS isolation (dB)	25	40	65
Intra-WSS isolation (dB)	45		
-0.5 dB passband width for 50 GHz channel (GHz)	32.3	33.0	35.6
-1.0 dB passband width for 50 GHz channel (GHz)	35.4	36.0	37.8
-3.0 dB passband width for 50 GHz channel (GHz)	42.1	42.8	43.2

TABLE II
The intrinsic loss of the WSSs

Component	Transmission	Passes	Loss (dB)
System components (Fresnel losses)	0.87	2	-1.21
DEMUX grating (Min/Max)	0.87/0.92	2	-0.72/-1.21
Intrinsic LCoS reflectivity	0.87	1	-0.60
Fibre coupling	0.85	1	-0.71
Total			**-3.24/3.73**

to 7.2 dB, with a median value of 5.96 dB. This insertion loss performance was comparable with the state of art [37], [38]. The fibre ports close to the optical axis of each WSS had lower insertion loss when compared with the outer ports. This is because the spatial frequencies of the beam steering holograms corresponding to these inner ports were lower. The LCOS device can achieve higher diffraction efficiency when displaying such holograms. The period of the blazed grating hologram for the port with the highest insertion loss was ~5 pixels. In this case, the diffraction efficiency of the LCOS device was at least reduced by 2 dB [39]. A theoretical breakdown of the intrinsic insertion loss of the WSSs is given in Table II. When the diffraction efficiency of the LCOS device is taken into account, the difference between the experimental and theoretical values is small and could be attributed to the misalignment of the system. The insertion loss performance of the two WSSs within the system was similar. This was expected since the optical arrangement for the two WSSs are mirrored. The overall insertion loss level shows that the primary aberrations in the relay optics have been successfully minimised. The conical diffraction effect from the highly dispersive GRISM has been kept as low as possible due to the use of the silicon prism in this work.

The polarisation dependent loss (PDL) was measured as <0.3 dB across the designed wavelength range. This is comparable with the state of art and further validated the polarisation diversity scheme implemented in this work.

B. Isolation

The port isolation within a WSS is defined as the ratio between the power at the target port to the power present at the un-targeted ports. During the characterisation process, the input optical beam was switched to an output port and the power levels at the rest of the output ports were measured individually. This process was repeated for all the output ports. Since the WSS port count was 35, there would be 34×35 =1190 port

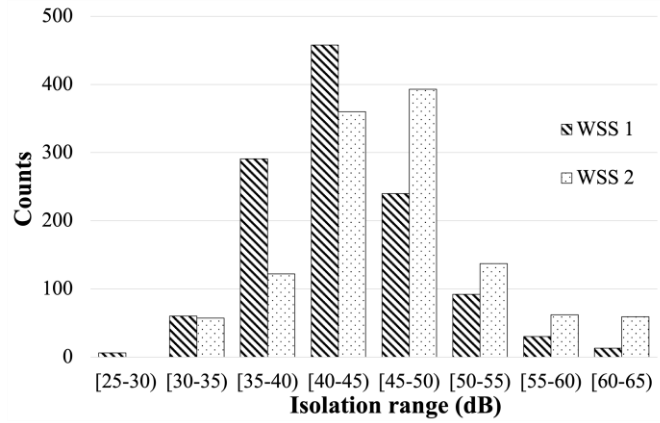

Fig. 6. Statistical distribution of the port isolation within each WSS.

isolation measurements to be carried out for each WSS in this work. Table I listed the worst-case, typical, and best-case port isolation level for our twin 1×35 WSS module. The statistical distribution of the isolation levels within each WSS was plotted in Fig. 6. The worst-case port isolation was measured as 25 dB. While majority of the instances exhibit an isolation level above 35 dB in both WSSs, the low isolation instances were primarily caused by the higher diffraction orders of the beam steering holograms displayed on the LCOS device. A wide variety of techniques have been demonstrated to further enhance the port isolation within a WSS, including the hologram optimisation [40]–[42], asymmetrical holographic optical architecture [43]–[45], etc. It should also be noted that the WSS 2 enjoyed a slightly better isolation level than WSS 1. This may be caused by the random scattering within the optical system or the residual spatial non-uniformity of the LCOS device [46].

The isolation between the WSSs within this module was >45 dB. This was mainly caused by the optical scattering.

C. Passband and Flexible Spectrum Switching

The passband performance was also measured in this work.

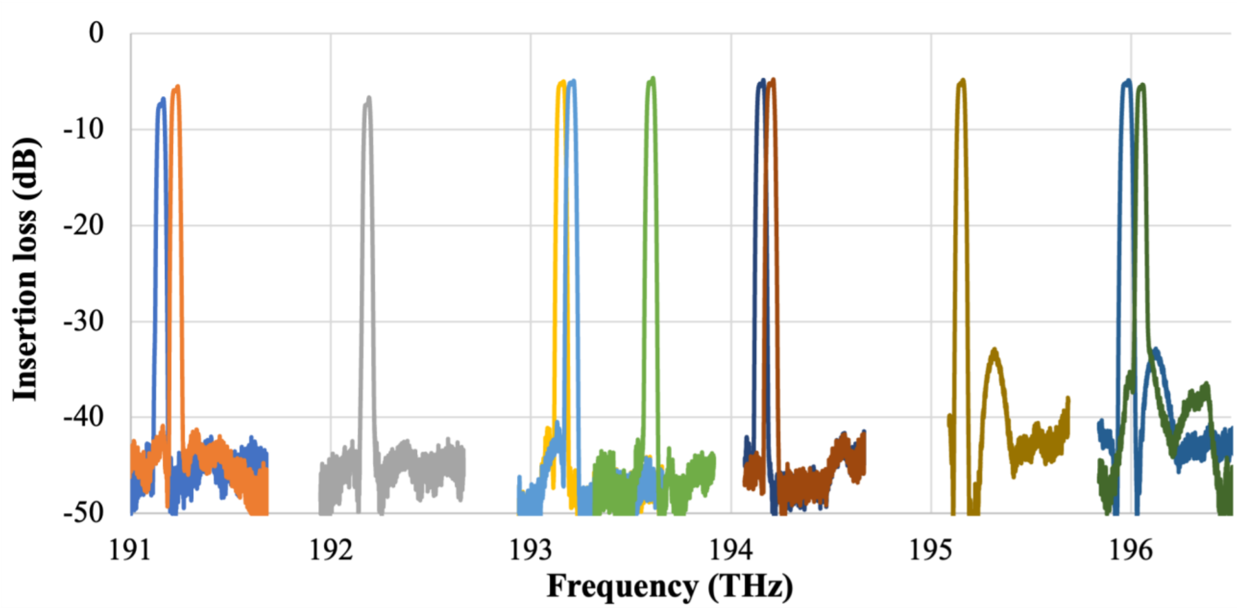

Fig. 7. Channelised switching across the designed spectral range.

Fig. 7 illustrated a typical channelised switching performance across 5 THz spectral range. It can be seen that the wavelength dependent loss was less than 2 dB across this spectral range. The operation of the flexible grid switching was demonstrated in Fig. 8. For a 50 GHz channel, the typical -0.5 dB passband width was 33 dB. There were some variations in the passband width across the spectral range. The detailed information was given in Table I. We also demonstrated ultra-wide band switching. Fig. 9 illustrated the passband performance for a 500 GHz channel. The passband ripple was <±0.1 dB across such a wide wavelength band.

In general, the experimentally measured passband performance was consistent with the theoretical model. This further validated our design, assembly and holographic control of this WSS module.

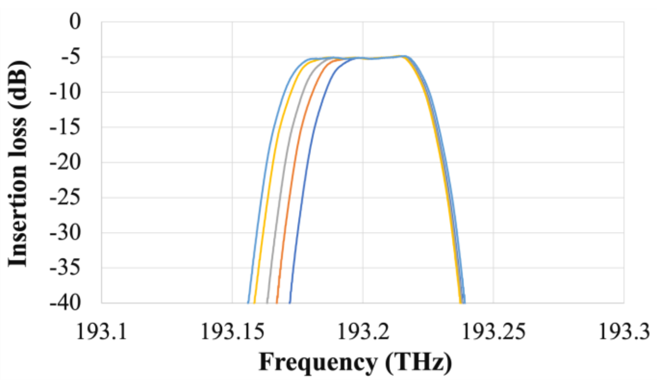

Fig. 8. The representative flexible spectrum switching performance.

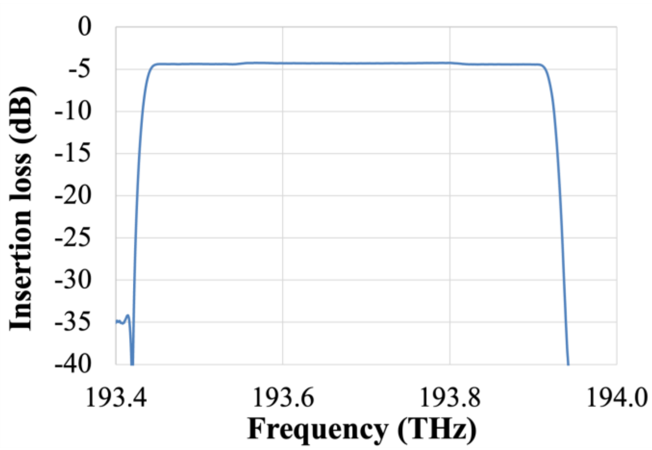

Fig. 9. Wide band channel switching capability

IV. Conclusion

This work demonstrated a compact twin 1×35 WSS module whose optical footprint was >50% smaller than the standard WSS module. The key enabling technology was a highly dispersive silicon GRISM with a dispersion capability of 0.30 degree/nm. The optical aberration, particularly the conical diffraction effect, caused by the diffraction grating with a groove density of 3200 lines/mm, was successfully minimised by the use of silicon prism in the GRISM structure and our optical design of the WSS systems. This was validated by extensive characterisations on the assembled WSS systems. Key performance metrics, including the insertion loss, PDL, isolation, passband, were measured. The results were comparable with the standard WSS modules. The 4f relay design adopted in this module was compatible with different switching optics configurations that may integrate an even higher number of WSSs. Therefore, this system can be easily reconfigured to support quad WSSs if required.

The footprint of the WSS optics is directly related to the cost of the WSS module. Therefore, the module demonstrated in this work is expected to have a significant cost advantage over the standard WSS modules. This may enable the WSS technologies to be widely deployed in the metro or even access networks that are more sensitive to the cost. On the other hand, the construction of a ROADM system is often constrained by the space available. The footprint reduction in the WSS modules would also help to increase the switching and port density of ROADM systems.

Further reduction of the footprint is possible by using even more dispersive GRISMs. However, the increased the groove density also will lead to fabrication challenges and higher cost. In addition, the effect of the conical diffraction discussed in Section II.C will also become more pronounced. This can potentially affect the performance of the WSS, particularly in terms of the insertion loss and passband.

References

[1] S. Frisken, S. B. Poole, and G. W. Baxter, "Wavelength-Selective Reconfiguration in Transparent Agile Optical Networks," Proceedings of the IEEE, vol. 100, no. 5, pp. 1056–1064, 2012.

[2] P. D. Colbourne and B. Collings, "ROADM Switching Technologies," 2011.

[3] S. Gringeri, B. Basch, V. Shukla, R. Egorov, and T. J. Xia, "Flexible architectures for optical transport nodes and networks," IEEE Communications Magazine, vol. 48, no. 7, pp. 40–50, Jul. 2010, doi: 10.1109/MCOM.2010.5496877.

[4] M. D. Feuer, D. C. Kilper, and S. L. Woodward, "8 - ROADMs and their system applications," in Optics and Photonics, I. P. Kaminow, T. Li, and A. E. B. T.-O. F. T. V. B. (Fifth E. Willner, Eds. Burlington: Academic Press, 2008, pp. 293–343. doi: https://doi.org/10.1016/B978-0-12-374172-1.00008-4.

[5] S. J. B. Yoo, Y. Yin, and K. Wen, "Intra and inter datacenter networking: The role of optical packet switching and flexible bandwidth optical networking," in 2012 16th International Conference on Optical Network Design and Modelling (ONDM), 2012, pp. 1–6. doi: 10.1109/ONDM.2012.6210261.

[6] A. Lord, Y. R. Zhou, R. Jensen, A. Morea, and M. Ruiz, "Evolution from Wavelength-Switched to Flex-Grid Optical Networks BT - Elastic Optical Networks: Architectures, Technologies, and Control," V. López and L. Velasco, Eds. Cham: Springer International Publishing, 2016, pp. 7–30. doi: 10.1007/978-3-319-30174-7_2.

[7] B. C. Collings, "Advanced ROADM technologies and architectures," in 2015 Optical Fiber Communications Conference and Exhibition (OFC), 2015, pp. 1–3. doi: 10.1364/OFC.2015.Tu3D.3.

[8] G. Baxter et al., "Highly programmable wavelength selective switch based on liquid crystal on silicon switching elements," 2006.

[9] T. Strasser and J. Wagener, "Wavelength-selective switches for ROADM applications," IEEE Journal of Selected Topics in Quantum Electronics, vol. 16, no. 5, pp. 1150–1157, 2010.

[10] D. M. Marom et al., "Wavelength-selective 1/spl times/K switches using free-space optics and MEMS micromirrors: theory, design, and implementation," Journal of Lightwave Technology, vol. 23, no. 4, pp. 1620–1630, 2005, doi: 10.1109/JLT.2005.844213.

[11] "https://www.lumentum.com/en/products/trueflex-twin-high-port-count-wavelength-selective-switch-twin-wss."

[12] "https://finisarwss.com/#products."

[13] H. Yang et al., "24 [1×12] Wavelength Selective Switches Integrated on a Single 4k LCoS Device," Journal of Lightwave Technology, vol. 39, no. 4, pp. 1033–1039, 2021, doi: 10.1109/JLT.2020.3002716.

[14] P. Wilkinson et al., "24 1×12 Wavelength-Selective Switches using a 312-Port 3D Waveguide and a Single 4k LCoS," in 2020 Optical Fiber Communications Conference and Exhibition (OFC), 2020, pp. 1–3.

[15] Y. Li, L. Gao, G. Shen, and L. Peng, "Impact of ROADM Colorless, Directionless, and Contentionless (CDC) Features on Optical Network Performance [Invited]," Journal of Optical Communications and Networking, vol. 4, no. 11, pp. B58–B67, 2012, doi: 10.1364/JOCN.4.000B58.

[16] L. Pascar, R. Karubi, B. Frenkel, and D. Marom, Port-reconfigurable, wavelength-selective switch array for colorless/directionless/contentionless optical add/drop multiplexing. 2015. doi: 10.1109/PS.2015.7328938.

[17] Y. Ikuma, K. Suzuki, N. Nemoto, E. Hashimoto, O. Moriwaki, and T. Takahashi, "8 × 24 wavelength selective switch for low-loss transponder aggregator," in 2015 Optical Fiber Communications Conference and Exhibition (OFC), 2015, pp. 1–3.

[18] K. Suzuki, K. Seno, and Y. Ikuma, "Application of Waveguide/Free-Space Optics Hybrid to ROADM Device," Journal of Lightwave Technology, vol. 35, no. 4, pp. 596–606, 2017.

[19] P. D. Colbourne, S. McLaughlin, C. Murley, S. Gaudet, and D. Burke, "Contentionless Twin 8×24 WSS with Low Insertion Loss," in 2018 Optical Fiber Communications Conference and Exposition (OFC), 2018, pp. 1–3.

[20] M. Blau and D. M. Marom, "Wavelength Demultiplexer Designs Operating Over Multiple Spatial Modes of a Rectangular Waveguide," IEEE Journal of Selected Topics in Quantum Electronics, vol. 26, no. 4, pp. 1–11, 2020, doi: 10.1109/JSTQE.2019.2909166.

[21] H. Chen, N. K. Fontaine, M. Mazur, R. Ryf, and D. T. Neilson, "Virtually Imaged Phase Array (VIPA)-Based Wavelength Selective Switch with High Spectral Resolution," in 2020 European Conference on Optical Communications (ECOC), 2020, pp. 1–4. doi: 10.1109/ECOC48923.2020.9333359.

[22] Z. Zhang, Z. You, and D. Chu, "Fundamentals of phase-only liquid crystal on silicon (LCOS) devices," Light: Science &Amp; Applications, vol. 3, p. e213, Oct. 2014.

[23] S. Frisken, G. Baxter, D. Abakoumov, H. Zhou, I. Clarke, and S. Poole, "Flexible and Grid-less Wavelength Selective Switch using LCOS Technology," in Optical Fiber Communication Conference and Exposition and The National Fiber Optic Engineers Conference, Technical Digest (CD), 2011, pp. 2–4.

[24] H. Yang and D. P. Chu, "Phase flicker in liquid crystal on silicon devices," Journal of Physics: Photonics, vol. 2, no. 3, p. 32001, 2020.

[25] H. Yang and D. P. Chu, "Phase flicker optimisation in digital liquid crystal on silicon devices," Optics Express, vol. 27, no. 17, pp. 24556–24567, 2019, doi: 10.1364/OE.27.024556.

[26] J. Nie, L. Dong, X. Tong, Y. Xu, W. Lin, and H. Yang, "Phase flicker minimisation for crosstalk suppression in optical switches based on digital liquid crystal on silicon devices," Optics Express, vol. 29, no. 7, pp. 10556–10567, 2021, doi: 10.1364/OE.415800.

[27] C. Pulikkaseril, L. a Stewart, M. a F. Roelens, G. W. Baxter, S. Poole, and S. Frisken, "Spectral modeling of channel band shapes in wavelength selective switches," Optics Express, vol. 19, no. 9, pp. 8458–70, Apr. 2011, [Online]. Available: http://www.ncbi.nlm.nih.gov/pubmed/21643096

[28] https://www.castech.com/product/Diffraction-Gratings-for-Telecommunication-73.html

[29] D. M. Marom, J. Dunayevsky, D. Sinefeld, M. Blau, R. Ryf, N. K. Fontaine, M. Montoliu, S. Randel, C. Liu, B. Ercan, M. Esmaeelpour, S. Chandrasekhar, A. H. Gnauck, S. G. Leon-Saval, J. Bland-Hawthorn, J. R. Salazar-Gil, Y. Sun, L. Grüner-Nielsen, and R. Lingle, "Wavelength-selective switch with direct few mode fiber integration," Opt. Express 23, 5723-5737 (2015)

[30] J. E. Harvey and C. L. Vernold, "Description of Diffraction Grating Behavior in Direction Cosine Space," Applied Optics, vol. 37, no. 34, pp. 8158–8159, 1998, doi: 10.1364/AO.37.008158.

[31] J. E. Harvey and R. N. Pfisterer, "Understanding diffraction grating behavior: including conical diffraction and Rayleigh anomalies from transmission gratings," Optical Engineering, vol. 58, no. 8, pp. 1–21, Aug. 2019, doi: 10.1117/1.OE.58.8.087105.

[32] S. Tibuleac and M. Filer, "Transmission Impairments in DWDM Networks With Reconfigurable Optical Add-Drop Multiplexers," Journal of Lightwave Technology, vol. 28, no. 4, pp. 557–568, 2010.

[33] T. Zami, B. Lavigne, and E. Balmefrezol, "Crosstalk analysis applied to Wavelength Selective Switches," in Optical Fiber Communication Conference and Exposition and The National Fiber Optic Engineers Conference, 2006, p. OFP4.

[34] H. Yang et al., "Impact of WSS Passband Narrowing Effect on the Capacity of the Flexible-spectrum Networks," in Optical Fiber Communication Conference, 2017, p. W1I.5. doi: 10.1364/OFC.2017.W1I.5.

[35] B. Robertson et al., "Application of the Fractional Fourier Transform to the Design of LCOS Based Optical Interconnects and Fiber Switches," Applied Optics, vol. 51, no. 12, pp. 2212–2222, 2012.

[36] Y. Ma et al., "Novel CDC ROADM Architecture Utilizing Low Loss WSS and MCS without Necessity of Inline Amplifier and Filter," in Optical Fiber Communication Conference (OFC) 2019, 2019, p. M1A.3. doi: 10.1364/OFC.2019.M1A.3.

[37] S. Yamamoto et al., "First demonstration of a C+L band CDC-ROADM with a simple node configuration using multiband switching devices," Optics Express, vol. 29, no. 22, pp. 36353–36365, 2021, doi: 10.1364/OE.433383.

[38] H. Yang and D. P. Chu, "Digital phase-only liquid crystal on silicon device with enhanced optical efficiency," OSA Continuum, vol. 2, no. 8, pp. 2445–2459, 2019, doi: 10.1364/OSAC.2.002445.

[39] H. Yang, P. Dolan, B. Robertson, P. Wilkinson, and D. Chu, "Crosstalk Spectrum Optimisation for Stacked Wavelength Selective Switches Based on 2D Beam Steering," in Optical Fiber Communication Conference, 2018, p. Th1J.2. doi: 10.1364/OFC.2018.Th1J.2.

[40] H. Yang, B. Robertson, and D. Chu, "Crosstalk Reduction in Holographic Wavelength Selective Switches Based on Phase-only LCOS Devices," in Optical Fiber Communication Conference, 2014, pp. Th2A-23.

[41] M. Nakajima et al., "Analysis and suppression of high-order diffractions in liquid-crystal-based spatial light modulator for photonic switch application," Japanese Journal of Applied Physics, vol. 56, no. 9S, p. 09NC01, 2017.

[42] B. Robertson et al., "The Use of Wavefront Encoding to Reduce Crosstalk in a Multicasting Fiber Telecom Switch," in Optical Fiber Communication Conference, 2012, p. OM2J.6.

[43] B. Robertson et al., "Reduction of crosstalk in a colourless multicasting LCOS-based wavelength selective switch by the application of wavefront encoding," in Proceedings of SPIE, 2012, vol. 8284, p. 82840S.

[44] H. Yang and D. P. Chu, "Transient Crosstalk in Holographic Optical Switching Based on Wavefront Encoding," Journal of Lightwave Technology, p. 1, 2019, doi: 10.1109/JLT.2019.2961193.

[45] Z. Zhang et al., "High quality assembly of phase-only liquid crystal on silicon (LCOS) devices," Journal of Display Technology, vol. 7, no. 3, pp. 120–126, 2011, Accessed: Oct. 30, 2011. [Online]. Available: http://www.opticsinfobase.org/abstract.cfm?URI=jdt-7-3-120